Influence of Pressure on Microbubble Production Rate in a Confined Turbulent Jet

D. R. Giosio[1], B. W. Pearce[1] and P. A. Brandner[1]

[1]Cavitation Research Laboratory, Australian Maritime College
University of Tasmania, Tasmania 7250, Australia

Abstract

The size spectra and production frequency of microbubbles generated within a confined turbulent jet from the expansion of supersaturated water are characterized by optical measurement. The generated microbubble plume is homogeneously dispersed into a uniform dilution flow before being discharged from a radial diffuser. Shadowgraphy measurements are made with a near range microscope on a 1 mm deep test volume at the outer radius of the diffuser eliminating depth of field limitations and allowing all detectable passing bubbles within the field of view to be imaged. The supersaturated water is expanded through a 0.5 mm diameter $\times$ 0.3 mm thick orifice plate into a 1.2 mm diameter expansion tube. The effect of tube geometry is investigated on two devices of 100 mm and 200 mm in length. Saturation water pressures ranging from 400 kPa up to 1200 kPa were tested. For all operating conditions the dominant size bubble was found to be between 10 to 15 μm while total production frequencies varied from 800 kHz up to 1200 kHz.

Introduction

There is ongoing interest in the use of micro- and nano-sized bubbles in a widening range of processes and applications such as: mineral processing [16] and waste water treatment; in medical applications for targeted drug delivery [7, 12] and contrast agents for medical imaging [14]; material synthesis [10]; and, for hydrodynamic research on cavitation and bubbly flows [1, 6, 9]. Microbubbles also introduce the possibility of providing soluble seeding for diagnostic techniques such as Particle Imaging Velocimetry (PIV) in water tunnels and other situations of transparent liquid flow [19].

In the hydrodynamic context, populations of minute bubbles naturally present in all practical volumes of water control the inception and dynamics of cavitation phenomena [3, 8]. These bubbles provide sites for nucleation and the inception of phase change. Such microbubbles or nuclei have a critical pressure, depending on diameter, below which their equilibrium is unstable undergoing rapid growth and hence complex macroscopic cavitation phenomena [2]. The critical pressure is always lower than the vapour pressure, decreasing with bubble diameter such that for small or micron sized bubbles large liquid tensions (negative pressures) are required for cavitation inception. With bubbly flows about marine vehicles more generally, there is also growing interest in the physics of microbubble formation and dispersion about the hull, propulsors and appendages [4, 11] whether from cavitation or other mechanisms [17, 20].

A diverse range of methods have been developed for the measurement of microbubble or nuclei spectra in test facilities [15]. Shadowgraphy is an optical technique that uses diffused pulsed backlighting to create shadows of bubbles or particles which are then captured with a high-resolution camera. An inherent issue with shadowgraphy is the depth of field limitation leading to uncertainties in detected particle size and number [5].

Various techniques for the generation of microbubbles have been developed for use in water tunnels [13]. The mini-tube type device investigated in the present study involves the expansion of water, supersaturated with dissolved air, through a sharp-edged orifice into a small diameter tube. Some limited data for this device has been published previously [2] though these results were affected by limitations of the set-up used. The present study seeks to improve and extend the characterization of the mini-tube type microbubble generating device. An improved experimental design has been implemented here to eliminate the depth of field limitation by imaging the flow discharged through a narrow radial diffuser. The bubble size spectra and production rate have been measured for a range of operating conditions and for two differing lengths of outlet tube.

Experimental Setup

Experiments were conducted in the variable pressure Cavitation Research Laboratory (CRL) Bubble Dynamics Chamber (BDC). The chamber, with a test volume of 520 mm $\times$ 520 mm $\times$ 1200 mm, was designed for investigating small-scale bubble and cavitation phenomena and has the same operating pressure range as the CRL water tunnel, from 4 to 400 kPa absolute. The chamber is constructed from 46 mm thick stainless steel plate with optical access through 1020 mm $\times$ 350 mm $\times$ 85 mm thick acrylic side windows and a 160 mm diameter acrylic port on the end plate. For the present study the top plate was replaced by a 10 mm glass sheet to enable the microscope to be positioned in close proximity to the test volume. A sketch of the experimental set-up is given in Figure 1.

The mini-tube microbubble generation device (see Figure 1) is centrally mounted within a vertical 70 mm OD $\times$ 8 mm thick acrylic circular section duct supplying a continuous dilution flow. A wire gauze and honeycomb section are located upstream of the generating device to provide a uniform low turbulence flow and ensure a homogeneous dispersion of the bubble plume within the duct. The combined dilution and bubbly plume flow is discharged from the duct via a radial diffuser. The measurement volume is positioned in the final 8 mm of the diffuser, which is parallel to and spaced 1 mm from, the interior surface of the top glass plate. A cone-shaped centre-body, aligned concentrically with the diffuser, was fitted to the glass plane to prevent a stagnation region forming where bubbles may collect and/or coalesce. Dilution flow is drawn from the chamber and recirculated via an ancillary circuit with the flow rate measured upstream of the chamber inlet using a Great Plains Industries Model 075E turbine meter with a precision of $< \pm0.5\%$.

Supersaturated water is supplied to the microbubble generator from a saturation vessel that may be pressurised up to 2000 kPa [2]. The saturation vessel pressure is measured using a Wika gauge pressure transducer Model P-10 with a precision of 0.1%. Atmospheric pressure is measured using a Vaisala Model PTB210 digital barometer with a precision of ±0.03 kPa. The volumetric flow rate of supersaturated water supplying the microbubble generator is calculated based on the time rate of change of water level in an isolated stand pipe using a Orion Instruments magnetically coupled liquid level sensor with precision of $< \pm0.5\%$.

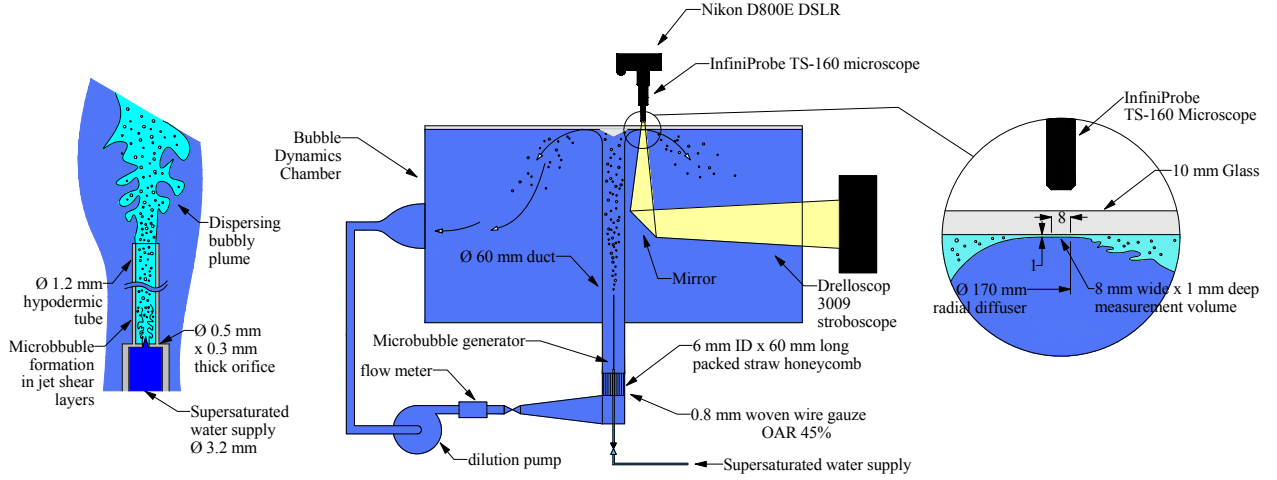Shadowgraph images were captured using a Nikon D800E

Figure 1: Schematic of experimental set-up of the Bubble Dynamics Chamber (BDC) for measurement of microbubble size and production rate. (Right) A magnified view of the measurement volume at radial diffuser outlet and (Left) Cross-section of mini-tube type microbubble generator.

DSLR and an InfiniProbe TS-160 continuously focusable microscope with MicroHM objective. The CMOS image sensor is 7360 × 4912 pixels with 14-bit optical resolution. A full field of view of 6.58 × 4.39 mm was used resulting in a spatial resolution of 0.89 μm/pixel with the required 1 mm depth of field. The camera and microscope objective were mounted to a LINOS X95 rail with a Melles Griot micrometre stage for precise positioning and fine adjustment of the focal distance. Backlighting was achieved using a Drelloscop 3009 strobe unit reflected off a 150 mm square polished mirror.

Experimental Procedure

Tests were conducted on two mini-tube type microbubble devices with differing expansion tube lengths – 100 mm and 200 mm, and for a range of operating conditions as described below.

The cavitation number, σ, for a microbubble generator may be defined, similarly as for a valve, as given by [13]:

$$\sigma = \frac{P_{down} - P_v}{P_{up} - P_{down}} \tag{1}$$

where P_{down} is the pressure at the microbubble generator outlet, P_v is the vapour pressure of the liquid at the test temperature, and P_{up} is the pressure just upstream of the microbubble generator orifice. Equation 1 may be expanded to give:

$$\sigma = \frac{\rho g h_w + P_{atm} - P_v}{(P_{sv} - P_L + \rho g \Delta h) - (\rho g h_w)} \tag{2}$$

where ρ is the density of water, g the gravitational acceleration, P_{atm} is the atmospheric pressure, P_{vap} is the vapour pressure, P_{sv} is the pressure of the saturation vessel, P_L is the head loss through the saturated water supply tube, Δh is the difference in elevation between the generator outlet and the level sensor reading, and h_w is the head of water in the chamber above the generator outlet.

Tests were performed with the BDC at atmospheric pressure while the saturation vessel pressure was varied from 400 kPa up to 1200 kPa giving $0.28 \leq \sigma \leq 0.09$. For all tests the dilution flow, Q_d, to saturation flow, Q_s, ratio was kept constant at approximately 50:1 to ensure adequate mixing and prevent any recirculating eddies forming within the circular duct. The nominal test conditions are presented below in Table 1.

Table 1: Nominal experimental conditions for both the 100 mm and 200 mm microbubble generator devices tested.

σ	0.28	0.18	0.14	0.11	0.09
P_{sv} (kPa)	400	600	800	1000	1200
Q_s (mL/s)	4.1	4.9	5.4	6.2	6.7
Q_d (L/s)	0.205	0.245	0.270	0.310	0.335

For each test condition data were acquired in 50 s periods, between which a significant settling time was observed to prevent microbubble recirculation through the dilution flow circuit. Pressure and flow measurements were acquired at 1 kHz while 100 images were captured for shadowgraphy analysis. A preliminary study performed on the same experimental set-up demonstrated converged statistics after approximately 50 images [18].

Shadowgraph images were post-processed in MATLAB to perform a background correction, to apply an adaptive contrast adjustment and cropped to give an effective field of view of 3.0 × 3.0 mm (i.e. a test volume of 9 mm^3). A sample image is given in Figure 2. Bubble detection and sizing was also performed in MATLAB using an algorithm implementing a circular Hough transform. The algorithm was applied over three size ranges to control the edge gradient threshold and sensitivity of detection required over the generated bubble size range to ensure accurate detections.

Detected bubbles were assigned to 5 μm size intervals. The production frequency, f_i, of bubbles in the ith 5 μm bin was calculated as:

$$f_i = (Q_d + Q_s)C_i \tag{3}$$

where C_i is the volumetric concentration of bubbles expressed as bubbles/mm^3, calculated based on the average number of bubbles per size range per image divided by the test volume.
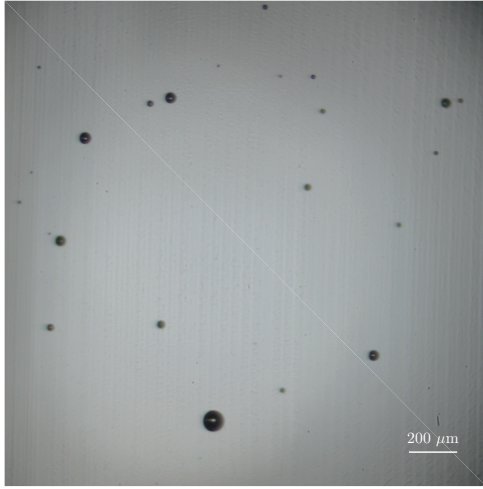
Figure 2: Sample backlit microbubble image taken at σ = 0.14, using the 100 mm tube length device.

Figure 3: Comparison of the production frequency between two different generator tube lengths at σ = 0.28. Data are presented as a histogram with a 5 μm bin width.

Results and Discussion

Key dimensionless parameters characterising the microbubble generator flow, namely, Reynolds number, $Re = U_j d/\nu$, Weber number, $We = \rho U^2 d/\gamma$, and discharge coefficient, C_D, are presented in Table 2 along with the total calculated production frequency given in units of kHz (where U_j is the generator jet mean velocity based on the orifice throat area, d is the orifice diameter, ν is the water kinematic viscosity, and γ is the water surface tension).

A comparison of the microbubble size spectra and production frequency for generators with 100 mm and 200 mm expansion tube lengths is given by the histogram presented in Figure 3. The bubble diameter is grouped in bins of 5 μm, plotted at the central bin value. The distribution shown in Figure 3 is for σ = 0.28, however this distribution is representative of all σ values tested as shown in Figure 4. For each value of σ, and expansion tube length, the dominant bubble size was found to be within the 10-15 μm range. Furthermore, the size distribution was found to be much broader for the shorter 100 mm expansion tube length device with a much greater proportion of detected bubbles within the 20-100 μm range. It is thought that the longer expansion tube length provides a greater opportunity for bubble breakup within the turbulent jet shear layers resulting in a much more uniform size distribution.

The total microbubble production frequency was found to vary from approximately 800 kHz at σ = 0.28 up to 1200 kHz at σ = 0.09 for both devices.

Conclusions

The influence of cavitation number and expansion tube length on the size distribution and production frequency of mini-tube type microbubble generators has been investigated. The experimental set-up used was designed to eliminate the need to perform depth of field corrections required with standard shadowgraphy measurements. Experimental results show that the dominant bubble size interval was 10-15 μm across the range of tested σ values and for both expansion tube lengths, however, a tighter size distribution was observed for the generator with the larger expansion tube length. The total production frequency was generally found to increase with decreasing σ with values ranging from ∼ 800 kHz up to ∼ 1200 kHz.
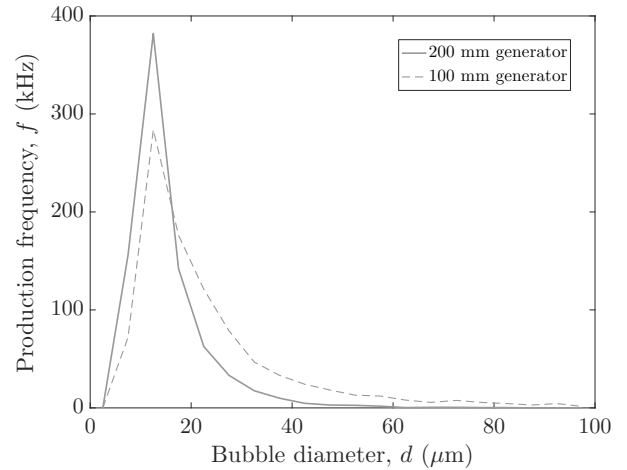
Table 2: Summary of relevant experimental parameters. Total microbubble production frequency, $f_{tot.}$ is given in units of kHz.

| Device | | Cavitation number, σ | | | | |
		0.28	0.18	0.14	0.11	0.09
100 mm	Re	8900	10500	11900	13300	14300
	We	3100	4300	5500	6800	7900
	C_D	0.76	0.74	0.73	0.72	0.71
	$f_{tot.}$	919	842	868	995	1080
200 mm	Re	8600	10300	11500	13100	14100
	We	2900	4200	5200	6700	7700
	C_D	0.76	0.72	0.72	0.71	0.70
	$f_{tot.}$	818	800	1100	1100	1170

References

[1] Brandner, P. A., Pearce, B. W. and de Graaf, K., Cavitation about a jet in crossflow, *Journal of Fluid Mechanics*, **768**, 2015, 141–174.

[2] Brandner, P. A., Wright, G., Pearce, B., Goldsworthy, L. and Walker, G. J., An Experimental Investigation of Microbubble Generation in a Confined Turbulent Jet, in *17th Australasian Fluid Mechanics Conference*, 2010.

[3] Brennen, C. E., *Cavitation and bubble dynamics*, Cambridge University Press, 2013.

[4] Castro, A. M. and Carrica, P. M., Bubble size distribution prediction for large-scale ship flows: Model evaluation and numerical issues, *International Journal of Multiphase Flow*, **57**, 2013, 131–150.

[5] Conrad, J., Depth of Field in Depth, Technical report, Large Format Photography, 2006.
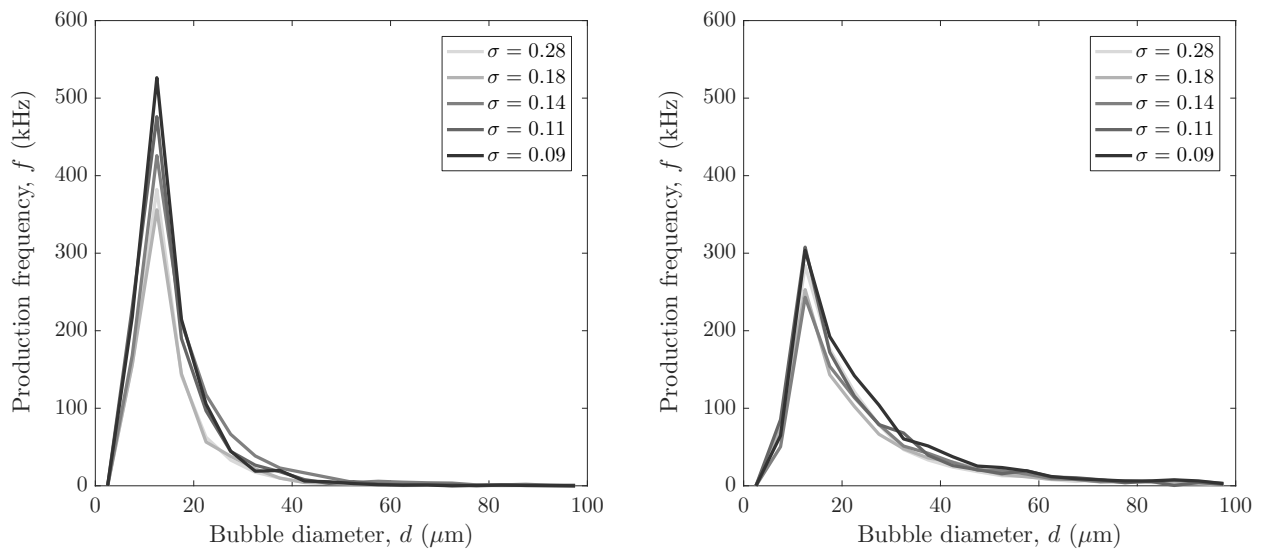
Figure 4: Production frequency histograms of the mini-tube microbubble generators across the range of tested cavitation numbers for an expansion tube length of 200 mm (left), and 100 mm (right).

[6] de Graaf, K. L., Pearce, B. W. and Brandner, P., The influence of nucleation on cloud cavitation about a sphere, in *ISROMAC16 - Sixteenth International Symposium on Transport Phenomena and Dynamics of Rotating Machinery*.

[7] Ferrara, K., Pollard, R. and Borden, M., Ultrasound microbubble contrast agents: fundamentals and application to gene and drug delivery., *Annual Review of Biomedical Engineering*, **9**, 2007, 415–447.

[8] Franc, J.-P. and Michel, J.-M., *Fundamentals of Cavitation*, Springer Science & Business Media, 2006.

[9] Gindroz, B. and Billet, M. L., Influence of the nuclei on the cavitation inception for different types of cavitation on ship propellers, *Journal of Fluids Engineering*, **120**, 1998, 171–178.

[10] Günther, A., Khan, S. a., Thalmann, M., Trachsel, F. and Jensen, K. F., Transport and reaction in microscale segmented gas-liquid flow., *Lab on a Chip*, **4**, 2004, 278–286.

[11] Jeon, D., Graff, E. and Gharib, M., Measurement of large scale bubbly flows, in *Proceedings of 27th Symposium on Naval Hydrodynamics*, Seoul, Korea, 2008.

[12] Klibanov, A. L., Microbubble contrast agents: targeted ultrasound imaging and ultrasound-assisted drug-delivery applications., *Investigative radiology*, **41**, 2006, 354–362.

[13] Lecoffre, Y., *Cavitation: Bubble Trackers*, A.A. Balkema, 1999.

[14] Lindner, J. R., Microbubbles in medical imaging: current applications and future directions., *Nature Reviews. Drug Discovery*, **3**, 2004, 527–32.

[15] Mées, L., Lebrun, D., Allano, D., Walle, F., Lecoffre, Y., Boucheron, R. and Fréchou, D., Development of interferometric techniques for nuclei size measurement in cavitation tunnel, in *28th Symposium on Naval Hydrodynamics*, 2010.

[16] Rodrigues, R. T. and Rubio, J., DAF dissolved air flotation: Potential applications in the mining and mineral processing industry, *International Journal of Mineral Processing*, **82**, 2007, 1–13.

[17] Russell, P. S., Giosio, D. R., Venning, J. A., Pearce, B. W., Brandner, P. A. and Ceccio, S. L., Microbubble generation from condensation and turbulent breakup of sheet cavitation, in *31st Symposium on Naval Hydrodynamics*, 2016.

[18] Trump, M. C., de Graaf, K. L., Pearce, B. W. and Brandner, P. A., An Experimental Investigation of the Optical Measurement of Microbubbles in a Confined Radial Jet, in *7th Australian Conference on Laser Diagnostics in Fluid Mechanics and Combustion*, Melbourne, Australia, 2015.

[19] van Overbrggen, T., Schrder, F., Klaas, M. and Schrder, W., A particle-image velocimetry tracer generating technique for liquid flows, *Measurement Science and Technology*, **25**, 2014, 087001.

[20] Washuta, N., Masnadi, N. and Duncan, J. H., The turbulent boundary layer on a horizontally moving,partially submerged, surface-piercing vertical wall, in *30th Symposium on Naval Hydrodynamics*, 2014.